Glioblastoma Pseudoprogression Discrimination Using Multiparametric Magnetic Resonance Imaging, Principal Component Analysis, and Supervised and Unsupervised Machine Learning

José Luis Thenier-Villa[1-3], Francisco Ramón Martínez-Ricarte[2,3], Margarita Figueroa-Vezirian[2], Fuat Arikan-Abelló[1-3]

■ BACKGROUND: **One of the most frequent phenomena in the follow-up of glioblastoma is pseudoprogression, present in up to half of cases. The clinical usefulness of discriminating this phenomenon through magnetic resonance imaging and nuclear medicine has not yet been standardized; in this study, we used machine learning on multiparametric magnetic resonance imaging to explore discriminators of this phenomenon.**

■ METHODS: **For the study, 30 patients diagnosed with IDH wild-type glioblastoma operated on at both study centers in 2011–2020 were selected; 15 patients corresponded to early tumor progression and 15 patients to pseudoprogression. Using unsupervised learning, the number of clusters and tumor segmentation was recorded using gap-stat and k-means method, adjusting to voxel adjacency. In a second phase, a class prediction was carried out with a multinomial logistic regression supervised learning method; the outcome variables were the percentage of assignment, class overrepresentation, and degree of voxel adjacency.**

■ RESULTS: **Unsupervised learning of the tumor in its diagnosis shows up to 14 well-differentiated tumor areas. In the supervised learning phase, there is a higher percentage of assigned classes ($P < 0.01$), less overrepresentation of classes ($P < 0.01$), and greater adjacency (55% vs. 33%) in cases of true tumor progression compared with pseudoprogression.**

■ CONCLUSIONS: **True tumor progression preserves the multidimensional characteristics of the basal tumor at the voxel and region of interest level, resulting in a characteristic differential pattern when supervised learning is used.**

INTRODUCTION

Glioblastoma is the most common primary malignant tumor in adults, accounting for approximately 60% of all gliomas.[1,2] The incidence of glioblastoma in Europe is about 3 per 100,000 inhabitants.[3,4] Even with current medical and therapeutic advances, median survival after diagnosis is 15–18 months and 5-year survival is only 5%, making it one of the diseases with a prognosis that remains almost universally fatal in the short term.[5]

Multiparametric magnetic resonance imaging (MRI) is the most useful noninvasive method for diagnosis and follow-up of glioblastoma, which (in most centers) includes at least 5 radiologic sequences considered relevant: T1-weighted imaging, gadolinium-enhanced T1-weighted, T2-weighted imaging, fluid-attenuated inversion recovery, and apparent diffusion coefficient. Each radiologic sequence has different pulse sequence characteristics,

Key words
- Glioblastoma
- Prediction models
- Principal component analysis
- Pseudoprogression
- Supervised learning
- Unsupervised learning

Abbreviations and Acronyms
MNLR: Multinomial logistic regression
MRI: Magnetic resonance imaging
PC: Principal component
PCA: Principal component analysis
ROI: Region of interest
SD: Standard deviation

From the [1]Department of Neurosurgery, University Hospital Arnau de Vilanova, Lleida, Spain; [2]Department of Neurosurgery, Vall d'Hebron University Hospital, Barcelona, Spain; and [3]Neurotrauma and Neurosurgery Research Unit (UNINN), Vall d'Hebron Research Institute (VHIR), Barcelona, Spain

To whom correspondence should be addressed: José Luis Thenier-Villa, M.D., M.B.I., Ph.D. [E-mail: jlthenier.lleida.ics@gencat.cat]

Citation: World Neurosurg. (2024) 183:e953-e962.
https://doi.org/10.1016/j.wneu.2024.01.074

*Journal homepage: **www.journals.elsevier.com/world-neurosurgery***

*Available online: **www.sciencedirect.com***

inversion time, or magnitude of diffusion of water molecules, which translates into different intensities for each tissue.[6]

Follow-up MRI is usually performed every 3 months after the first radiologic imaging study. In some patients, the combination of chemoradiation therapy produces significant radiologic changes during the first 3–6 months of treatment, and a phenomenon called pseudoprogression occurs in between 36% and 50% of cases,[7] simulating a tumor progression in MRI, with a characteristic increase or appearance of new areas of contrast enhancement compared with early postoperative MRI, and constituting a challenge in the follow-up of glioblastoma, because only the biopsy or late radiologic findings are conclusive of true progression, and their inadequate classification can lead to delayed treatment of true progression, or inappropriate therapeutic escalation in cases of pseudoprogression.[8-10]

A recent review[11] addressed the different radiologic and nuclear medicine solutions proposed for the discrimination of pseudoprogression and true tumor progression. The investigators concluded that advanced MRI and positron emission tomography seem superior for this purpose; however, uniform and standardized practices or protocols, which allow reproducibility between different populations, are lacking. In that review, biomedical informatics methods for voxel-level multidimensional data transformation with machine learning algorithms are not mentioned as an explored technique. Feature extraction and redundancy removal from multispectral images have rarely been used in brain tumor MRI analysis but have been found useful for classification purposes in normal brain tissue and tumors from other locations.[12,13]

METHODS

Study Population

For this study, 60 brain MRI studies from 30 patients were analyzed, obtained from the brain tumor database of the University Hospital Arnau de Vilanova in Lleida, Spain and Vall d'Hebron University Hospital in Barcelona, Spain (2011–2020). For this study, we included patients with histologic confirmation of IDH wild-type glioblastoma by surgical resection with a minimum follow-up of 9 months and at least 2 late postsurgical MRI studies (3–6 months). We explicitly excluded patients with absence of adjuvant treatment for any reason; significant postsurgical complications including hematomas, infections, or infarctions; age >75 years; biopsy only; and patients under clinical trial or who had received a different treatment from the standard.

Fifteen cases corresponded to patients with a diagnosis of early postsurgical tumor progression and 15 cases corresponded to patients with a diagnosis of pseudoprogression, confirmed by clinical-radiologic evolution or biopsy. Two MRIs obtained at 2 different times (diagnosis and progression/pseudoprogression report) were analyzed in the same multidimensional space. This study design was approved by the medical research ethics committee of the University Hospital Arnau de Vilanova (CEIC-2774) and University Hospital Vall d'Hebron (PR(AG)25/2023).

Principal Component Analysis

Principal component analysis (PCA) is a multivariate analysis method that allows assessing multidimensional datasets (in this study, each MRI sequence corresponds to 1 dimension), for which linear combinations of the original variables that represent the greatest variability of the data are sought. An application of this technique is the reduction of dimensionality, so that when there is a large number of possibly correlated variables (the physical characteristics of the tissue define its behavior in each MRI sequence), it allows reducing them to transformed variables, called principal components (PCs), that explain all the variability of the data.[14] Each PC is obtained by a linear combination of the original variables, which can be understood as new variables obtained by combining the original variables in a certain way. The process to follow to calculate the first PC is:

- Histogram-matching normalization for each pair of sequences of the 5 MRI sequences of interest (diagnostic and follow-up pair of sequences) so different machine acquisitions become comparable.[15]
- Centering of the variables: the mean of the variable to which it belongs is subtracted from each value. This process ensures that all variables have zero mean, so different MRI sequences become comparable.
- An optimization problem is solved to find the value of the loadings with which the variance is maximized computing the eigenvector-eigenvalue of the covariance matrix.

Once the first component (PC1) has been calculated, the second (PC2) is calculated by repeating the same process, with the condition that the linear combination cannot be correlated with the first component. This process is equivalent to saying that PC1 and PC2 have to be perpendicular (uncorrelated). The process is repeated iteratively until 5 PCs are calculated (the same number as there are sequences). The order of relevance of the components is given by the magnitude of the variance explained by each component.[16]

If all the PCs of a dataset are calculated, then, although transformed, all the information present in the original data is being stored.

Unsupervised Learning

The clustering method corresponds to the field of unsupervised learning; in this machine learning technique, data delivered to the algorithm have not been previously categorized by their origin or by human intervention (unlabeled data). Clustering was shown to be more efficient for segmentation when there is no data redundancy and, hence, the relevance of PCA as a previous step.[17]

In k-means clustering, it is assumed that there are many groups from a dataset; the number of groups is defined as k, hence, the name of the algorithm. The task of the algorithm is to define to which type of category (cluster) each data point belongs (in our case, each MRI voxel after PCA). The objective is the search for cluster centers that minimize the intracluster variance by minimizing the square of the euclidean distance between a cluster center for all the components of that cluster.

The standard algorithm includes a series of iterative refinements from naive k-means random centers (initialization) so that in each iterative step the mean or centroid is recalculated for

the observations assigned to a cluster. The algorithm converges when after reassigning the centroids, the components no longer show changes.[18]

In our study, we used a maximum of 600 iterations and a range of centroids from 2 to 20. The optimal number of centroids was obtained through the statistical gap method following the criteria of Tibshirani et al.[19] The clustering labels are then returned to the transformed data matrixes preserving their spatial origin and are graphically represented in the same spatial frame.

A set of single-class voxels does not obey only the multidimensional clustering criterion; the second criterion, spatial adjacency of the voxel classes, was analyzed using congruence comparison in adjacency matrixes. A neighborhood matrix for 4 directions was obtained with the function raster:adjacent in R (R Foundation for Statistical Computing, Vienna, Austria). The minimum valid criterion was 50% of adjacency (this means that any voxel should be adjacent to another voxel with the same class in at least 50% of cases to become a true cluster). In cases of low adjacency, the procedure was repeated, decreasing k to k−1 until the minimum allowed adjacency of 50% was reached.

Supervised Learning

Once the multidimensional voxels in the preoperative brain MRI have been clustered, the supervised learning method on the follow-up MRI is used to assign each new voxel of the region of interest (ROI) to the identified groups training the model with the unsupervised phase data. In our study, multinomial logistic regression (MNLR) was used. MNLR is a statistical classification algorithm, an extension of binary logistic regression to multiclass classification problems on multidimensional data[20] (the optimal number of k from the previous step is the number of voxel classes for this task), and it consists of 2 layers: a predictive linear function (logit layer) and a softmax function (softmax layer). The result of the supervised prediction is transferred to the transformed data matrixes preserving their spatial origin and predicted clusters are represented using color scales.

To evaluate the supervised learning task in this study, we used as indicators the percentage of assigned classes (quotient of the total classes assigned and the total number of clusters obtained in the unsupervised phase for the same case; any assigned class should represent at least 5% of the ROI, otherwise it is classified as not valid), the number of classes overrepresented (i.e., the number of classes with an assignment >150% in reference to the same class from the unsupervised phase), and the degree of voxel adjacency from the classes predicted.

Data Treatment

MRI acquisitions included the following manufacturers: MRI 1.5 T (Ingenia [Philips Healthcare, Best, The Netherlands]); MRI 1.5 T (Gyroscan Intera [Philips Systems, Best, The Netherlands]), Magnetom Avanto 1.5 T (Siemens, Erlangen, Germany) and Trio 3T (Siemens, Erlangen, Germany).

The raw DICOM (Digital Imaging and Communications in Medicine) data from hospital PACS (picture archiving and communication system) was pseudonimized following the institutional protocol and, then, 3 phases of the data proceeded as follows (Figure 1).

- Registration and reformatting: The process consists of aligning multiple images with the aim of ensuring an anatomic spatial correspondence of the intracranial space. For this process, the general registration module BRAINS of 3D Slicer 4.11 (Brigham and Women's Hospital, Boston, Massachusetts, USA) was used reformatting to 200 slices, 320 × 320 pixels, and 0.75-mm spacing. After the procedure, 8 datasets were obtained, 5 derived from sequences, 1 mask including only brain area and 2 including specific tumoral masks segmented with threshold tools and validated by the authors (postsurgical residual tumor areas were excluded from progression/pseudoprogression ROI).
- Brain extraction: For this process, the Swiss Skull Stripper tool of 3D Slicer was used, creating a single mask based on the T1 sequence with 3D contrast (volumetric).
- Analysis with R in RStudio environment: consisting of the sequential use of the following libraries and tools: oro.dicom, EBImage, Ggplot2, RStoolbox, raster, rasterPCA, RStoolbox::-histMatch, moments, nnet, Seurat, NbClust, among others.

Statistical Analysis

The outcome variables measured in the study and obtained in the supervised learning phase are the percentage of assigned classes, the number of overrepresented classes, and the global adjacency of voxels of the same class. For the contrast of quantitative variables, the nonparametric Mann-Whitney U test was used.

Gross total resection is defined as a full complete resection of the enhancing tumor, near-total resection is defined as 95%−99% of resection of the enhancing tumor and residual tumor <1 cm^3, and subtotal resection is defined as 80%−94% of extent of resection of the enhancing tumor.[21]

RESULTS

Demographic Characteristics of the Population

For this study, 30 patients were included; 19 patients (63%) were male and 11 patients (39%) were female, and the average age of the patients was 58 years. Most patients were clinically stable at the time of the progression/pseudoprogression MRI diagnosis (23/30 cases); 2 patients from the pseudoprogression group and 5 from the progression group were clinically worsening by the time of the second MRI according to medical records. In our subset of patients included in this study, in which only-biopsy intended, elderly patients, and IDH-mutant tumors were excluded, the extent of resection achieved was 70% for gross total resection, 27% for near-total resection, and 3% for subtotal resection.

Other baseline characteristics of the population including gender, age, volume, and survival by groups are summarized in Table 1.

PCA

After applying the PCA by pairs of MRI studies under the same spatial framework, the PCs are obtained, which results in the same number of datasets as sequences used in the study. Each PC represents an uncorrelated distinguishable feature of the MRI signal. A sample case is shown in Figures 2 and 3, when using RGB (red, green, blue) model for colors, 1 channel for each PC; the feature selection function is shown. PCA data for all

components were used in both the supervised and the unsupervised machine learning phase.

Clustering of the ROI

For the 30 cases, the optimal number of clusters obtained has a mean of 9.37 (range, 5–14; standard deviation [SD], 2.7); there was no difference in the number of clusters of the diagnostic MRI for the progression group (9.12; SD, 2.60) and pseudoprogression group (9.33; SD, 2.73) ($P = 0.51$, Mann-Whitney U test). This phase required convergence from k to k–1 for 8 patients (3 patients in the progression group and 5 patients in the pseudoprogression group) because of noncompliance with the spatial segregation criterion.

Supervised Learning

The voxel category prediction phase was performed using MNLR. The indicators of the comparative findings of progression and pseudoprogression are summarized in **Table 2**. There is a greater number of assigned classes, fewer overrepresented classes, and greater adjacency in the true tumor progression group. The lesion volume in cases of true tumor progression was also greater (13.55 and 8.66 cm^3 for the progression and pseudoprogression groups, respectively; $P = 0.01$, Mann-

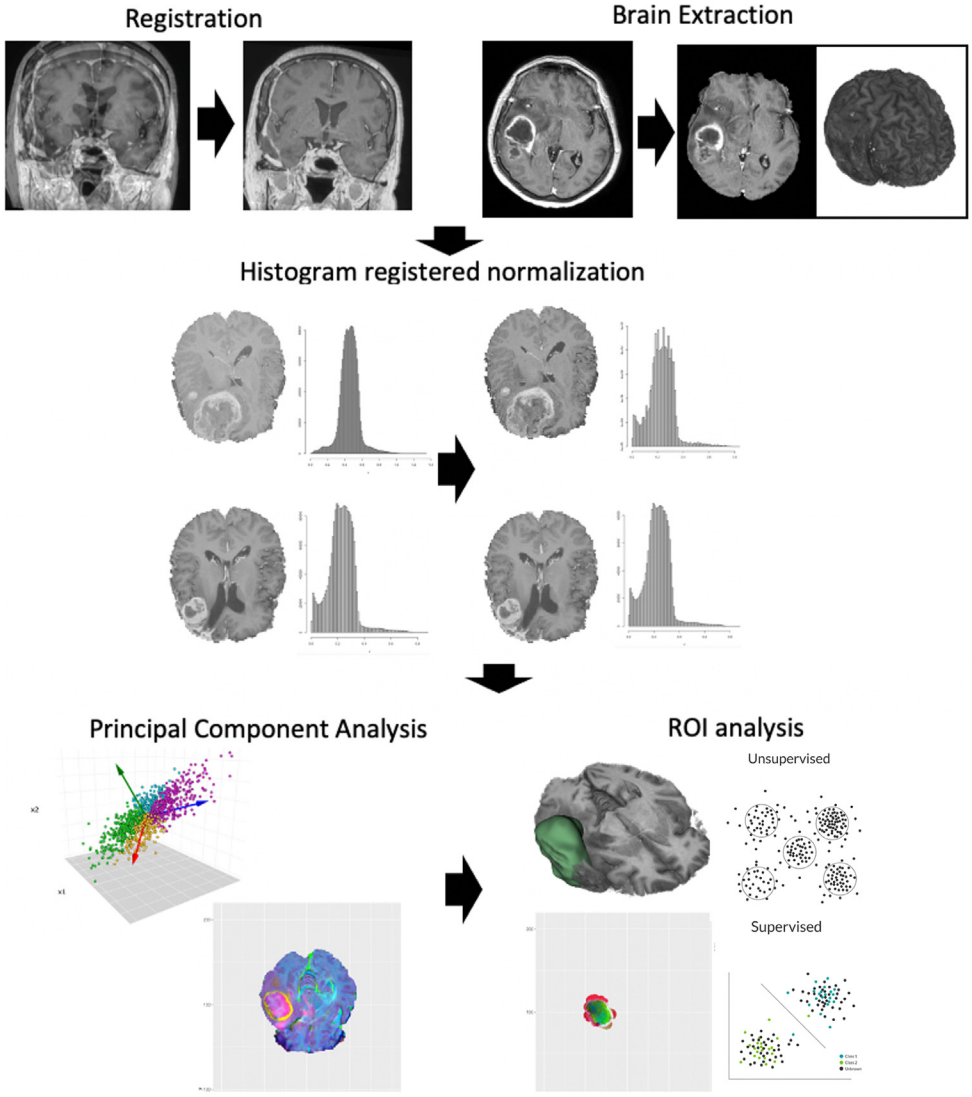

Figure 1. Steps for processing RAW image to principal component analysis image assessment: Registration of multiple sequences and multiple acquisitions of magnetic resonance imaging, brain extraction applied, normalization using histogram-matching approach, principal component analysis and region of interest (*ROI*) analysis.

Table 1. Baseline Characteristics of the Study Population

	Progression (n = 15)	Pseudoprogression (n = 15)
Age (years), mean (SD)	60.83 (9.95)	55.35 (11.72)
Gender (male/female)	9:6	10:5
Initial tumor volume (cm^3), average (SD)	27.55 (8.23)	30.12 (10.76)
Progression/pseudoprogression volume (cm^3), average (SD)	13.55 (3.55)	8.66 (2.12)
Overall survival (months), average (SD)	18.91 (8.32)	24.38 (10.34)
Symptomatic worsening previous to second magnetic resonance imaging, n (%)	5/15 (33)	2/15 (13)
Gross total resection/near-total resection/subtotal resection (n)	10/4/1	11/4/0

SD, standard deviation.

Whitney U test). Significance was established by Mann-Whitney U test.

DISCUSSION

Glioblastoma multiforme takes its name "multiforme" from its heterogeneous nature. Glioblastomas are formed by tumor cells that differ in their morphology, genetics, and biological behavior, which highlights their ability to resist conventional therapies that have a strong impact on the patient's prognosis.[22-24] Studies of heterogeneity in contrast-enhanced T1 sequences have shown a correlation with the survival prognosis of patients.[25]

Tumor progression of a glioblastoma arises as a new area of contrast enhancement or the growth of a known residual enhancing tumor, an indistinguishable feature of the process called pseudoprogression, present in up to 50% of patients.[26,27] Contrast enhancement of intracranial lesions is mainly caused by the rupture of the blood-brain barrier, a nonspecific phenomenon of tumor activity found in other processes such as infections or inflammatory diseases.[26,28,29] In pseudoprogression, the phenomena

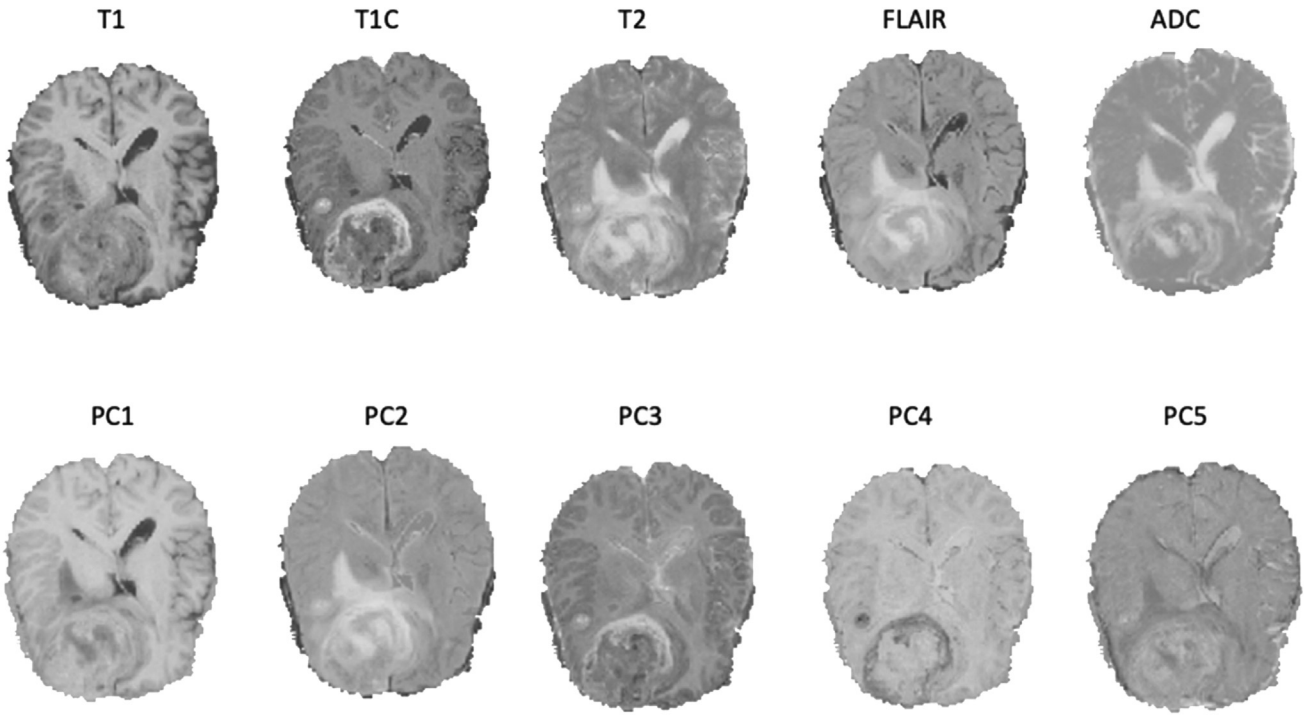

Figure 2. Sample case of temporal glioblastoma. Top row, from left to right: T1-weighted imaging (T1), contrast-enhanced T1-weighted imaging (T1C), T2-weighted imaging (T2), fluid-attenuated inversion recovery (FLAIR), apparent diffusion coefficient (ADC). Bottom row, from left to right: principal component 1 (PC1), PC2, PC3, PC4, and PC5.

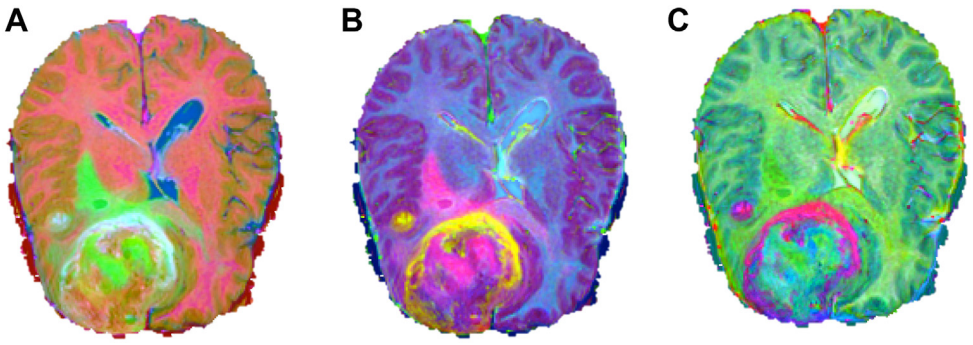

Figure 3. RGB plots: sample case of temporal glioblastoma. RGB plot from principal components: (**A**) RGB plot for P1-PC3 (*red*, PC1; *green*, PC2; *blue*, PC3). (**B**) RGB plot for PC2-PC4 (*red*, PC2; *green*, PC3; *blue*, PC4). (**C**) RGB plot for PC3-PC5 (*red*, PC3; *green*, PC4; *blue*, PC5).

that induce this increase in contrast enhancement are not fully understood and could include an increase in vascular permeability induced by hypoxia in relation to temozolamide,[26] vascular endothelial cell death secondary to radiation therapy, or interaction of complex processes (inflammation, apoptosis, vascular hyalinization, release of cytokines) without the accumulation or proliferation of glioblastoma tumor cells.[26]

Although the study of tumor progression focuses on the T1 sequence after intravenous gadolinium contrast administration, studies carried out on T2 sequences have shown notable differences in the degree of tumor heterogeneity.[25,30] In addition, tumor progression is also accompanied by changes in the signal of T2 and fluid-attenuated inversion recovery sequences.[7] In conventional MRI sequences, contrast enhancement alone does not seem to be a specific discriminator of pseudoprogression; other sequences such as diffusion and perfusion seem to perform better,[7,31] highlighting the nature of different cellularity and blood dynamics for both processes.[32] Several studies have shown that apparent diffusion coefficient values (which inversely correlate with diffusion-weighted images) are lower in recurrent tumors than in radiation injuries,[33-35] probably because of the characteristic of greater cellularity of tumor lesions. Cellularity is associated with reductions in the extracellular space that lead to decreased diffusion of water molecules.[36] Although this characteristic is useful within the contrast-enhanced areas, other tumoral areas such as cystic or necrotic areas have different behaviors in diffusion.[37,38] Because multiple and redundant characteristics are found in different MRI sequences, multidimensional transformation with feature extraction using PCA helps to analyze and differentiate voxel-level characteristics on neuroimaging.

In our study, we generated 5 new datasets using PCA, which, being decorrelated, better represents differentiated cell populations or physical characteristics of the tissues. Unsupervised learning has shown usefulness for segmentation of tumors from normal brain parenchyma,[39,40] and, therefore, a highly heterogeneous tumor such as glioblastoma could be segmented using the same principle and same statistical method. Moreover, determination of the optimal number of intratumoral voxel populations by a gap statistic method can be useful to represent multiclonality in radiologic studies, and it is an aspect that we have not found in previous glioblastoma MRI studies, but it is recognized as a measure of heterogeneity and is widely studied in gene-expression studies.[41]

Contrary to the classic description of 3 glioblastoma zones (cystic, necrotic, and solid),[42] in our study, we found that multidimensional clustering by k-means can find up to 14 well-differentiated tumor zones, confirmed by the adjacency criterion (a high degree of voxel neighborhood from the same cluster), which does not seem to be a simple statistical noise. In the supervised learning phase using MNLR, patients with tumor progression present with better class assignment, exceeding 90% of the volume in most cases, with fewer overrepresented classes and a higher degree of voxel adjacency. On the other hand, in pseudoprogression, which is less heterogeneous,

Table 2. Supervised Learning Class Prediction Indicators on Magnetic Resonance Imaging from Progression and Pseudoprogression Region of Interest Analysis

	Progression (n = 15)	Pseudoprogression (n = 15)	*P* Value
Percentage of assigned classes, mean (SD)	95.34 (12.22)	34.45 (7.62)	<0.01
Number of overrepresented classes, mean (SD)	0.22 (0.1)	2.2 (0.3)	<0.01
Global voxel class adjacency (%)	55.12	33.53	

SD, standard deviation.

the task is solved generating an excess of assignments to a specific class (overrepresenting), with a low degree of voxel adjacency and lower occupation of all the classes to predict.

All these findings suggest that the tumor recurrences (true progression) retain similar characteristics in its multidimensional intensities compared with the baseline tumor. Pseudoprogression presents more homogeneous populations with less variance and more restricted populations compared with the baseline tumor. Machine learning techniques showed usefulness for predicting pseudoprogression at a voxel/ROI level. Representative sample cases are presented in Figures 4 and 5.

As limitations of the study, issues arising when comparing different brain magnetic resonance images are well described in the literature. Various studies use different methods of registration and brain extraction,[43,44] which generate differences in datasets. The normalization method between MRI is also relevant (e.g., RAVEL [Removal of Artificial Voxel Effect by Linear Regression], WhiteStripe, histogram matching, z-score),[45] and no method has shown superior performance in brain tumors. In our study, we used the histogram-matching method, which seems to have better performance in neoplastic lesions from other locations,[46] and we avoid using methods based on maximum-minimum and methods referenced in white matter, because brain edema, tumor infiltration, and gadolinium enhancement can generate large deviations and distant outliers in intensities from one acquisition to another. Despite the potential limitations of the technique, our data performed well with the technique used.

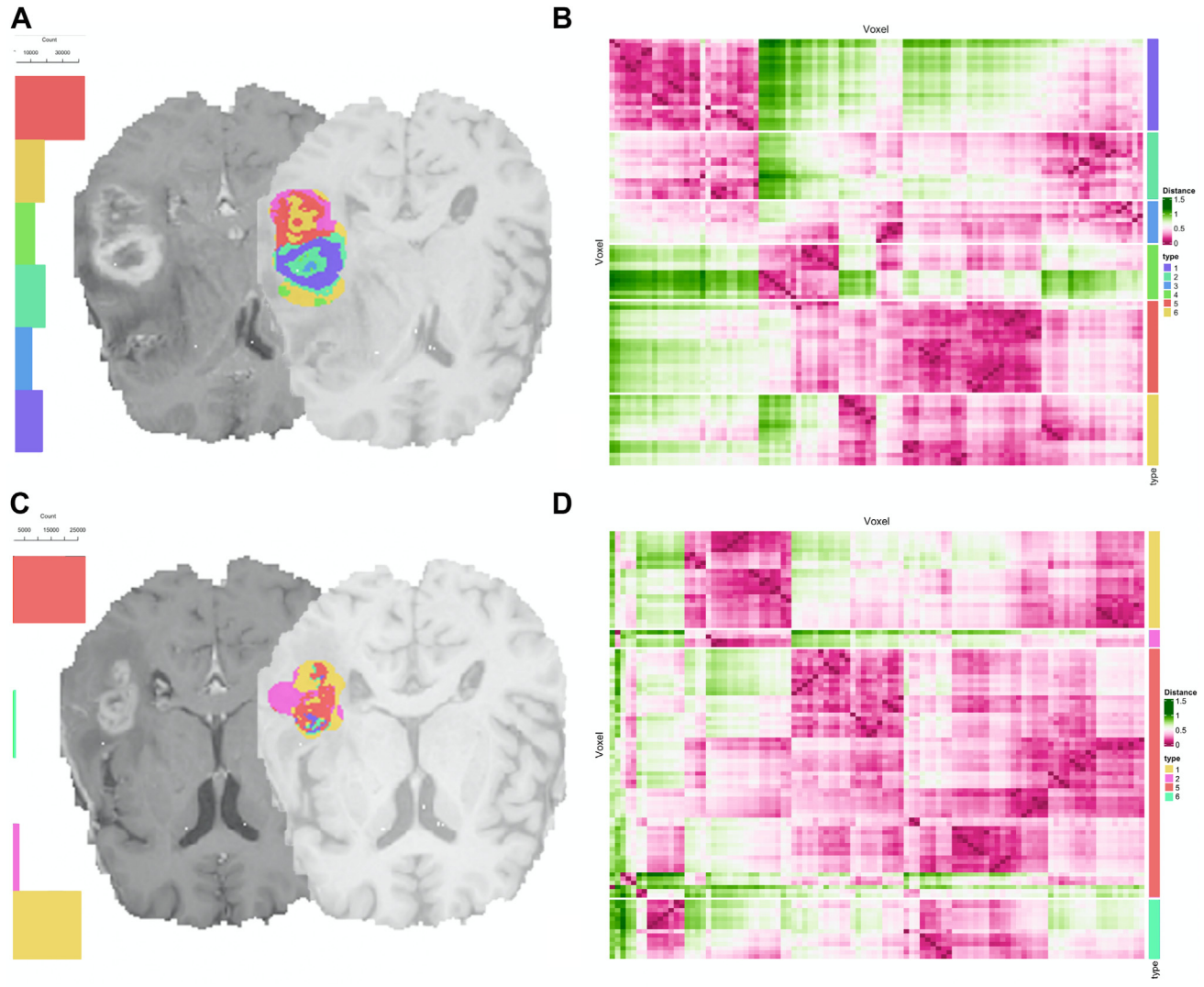

Figure 4. Sample case of tumor pseudoprogression. (**A**) Baseline tumor showing 6 tumor zones. (**B**) Heatmap of voxel-pairwise-distances from tumor region. (**C**) Pseudoprogression showing 2 of 6 predicted classes (both overrepresented). (**D**) Heatmap of voxel-pairwise-distances from pseudotumor region showing less heterogeneity and 1 large cluster and 3 small clusters.

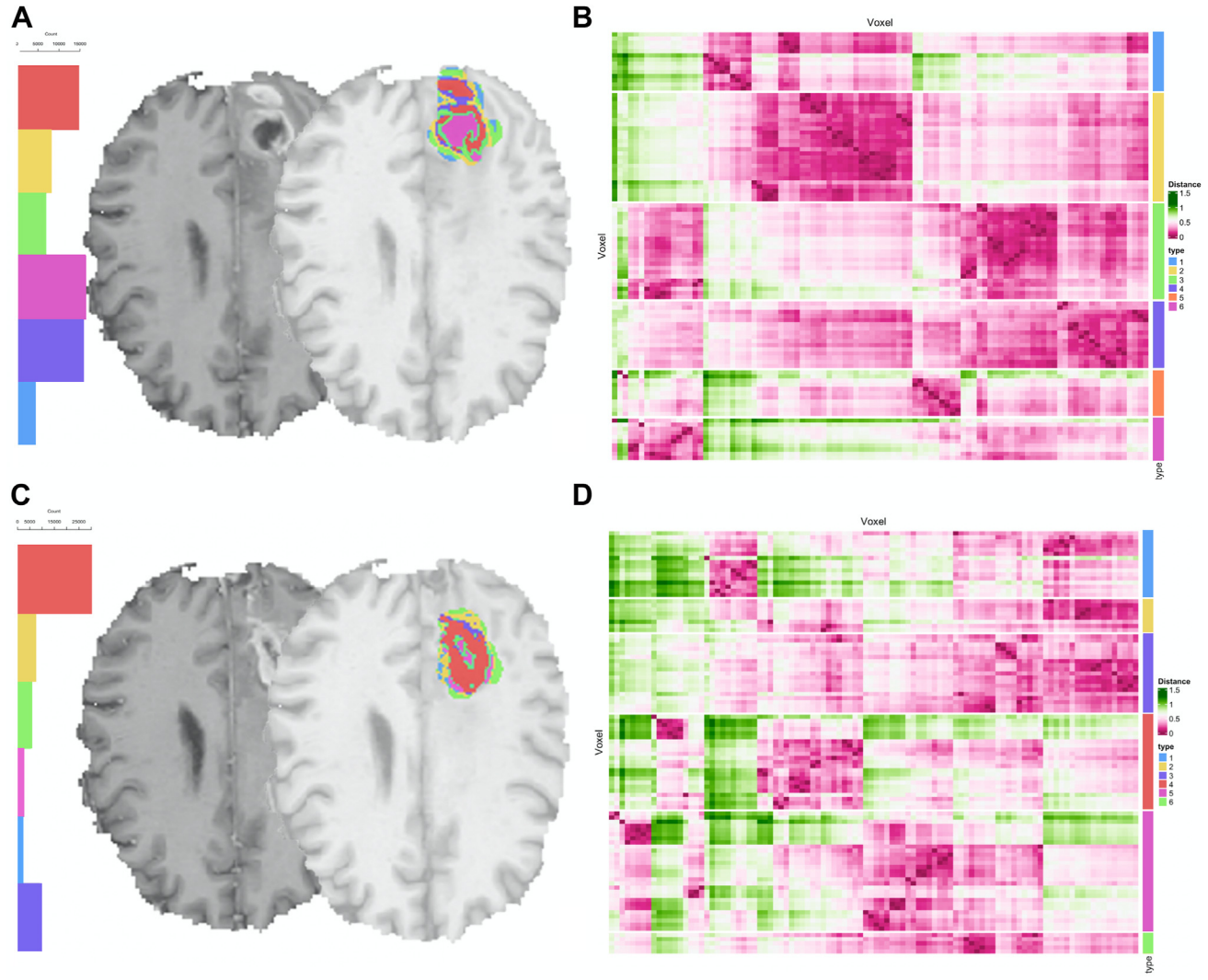

Figure 5. Sample case of tumor progression. (**A**) Baseline tumor showing 6 tumor zones. (**B**) Heatmap of voxel-pairwise-distances from tumoral region. (**C**) True progression showing 6 of 6 predicted classes. (**D**) Heatmap of voxel-pairwise-distances from tumoral region showing multiple well-distributed clusters.

In addition, the small number of cases constitutes a limitation in our study. The search for homogeneity of the cases in search of consistent results necessitates performing multicenter studies, which will allow analysis to be carried out in more variables including extent of resection, survival, and response to specific treatments in addition to analysis of astronomic numbers of voxels. Moreover, as the amount of processable information increases in hospital datasets, studies will require a higher computational effort, making it necessary to create high-level processing and storage servers to conduct higher-quality studies.

CONCLUSIONS

- Brain MRI with PCA and machine learning techniques allow effective discrimination of tumor and pseudotumor at a voxel/ROI level.
- Unsupervised clustering of glioblastoma showed a high degree of heterogeneity with up to 14 well-differentiated tumoral areas.
- Tumoral progression preserves most of the multidimensional characteristics from the baseline tumor, which results in a

characteristic differential pattern when an MNLR task is used to solve the supervised learning problem.

CRediT AUTHORSHIP CONTRIBUTION STATEMENT

José Luis Thenier-Villa: Formal analysis, Investigation, Methodology, Software, Visualization, Writing — original draft, Writing — review & editing. **Francisco Ramón Martínez-Ricarte:** Data curation, Methodology, Validation, Writing — original draft, Writing — review & editing. **Margarita Figueroa-Vezirian:** Data curation, Investigation, Writing — original draft, Writing — review & editing. **Fuat Arikan-Abelló:** Project administration, Resources, Supervision, Validation, Writing — original draft, Writing — review & editing.

ACKNOWLEDGMENTS

We thank our colleagues, neurosurgeons, radiologists, pathologists, oncologists, anesthetists, intensivists, residents, nurses and to all the personnel of Hospital Universitari Arnau de Vilanova and Hospital Universitari Vall d'Hebron, for being always dedicated to the care of our most vulnerable patients. Establishment of a new organization and a high-level collaborative scheme between both centers of the Institut Català de la Salut has allowed us, despite the distance, to share and unify the clinical and research experience to the benefit of our patients and society.

REFERENCES

1. Ostrom QT, Gittleman H, Stetson L, Virk SM, Barnholtz-Sloan JS. Epidemiology of gliomas. *Cancer Treat Res*. 2015;163:1-14.
2. Ahmed R, Oborski MJ, Hwang M, Lieberman FS, Mountz JM. Malignant gliomas: current perspectives in diagnosis, treatment, and early response assessment using advanced quantitative imaging methods. *Cancer Manag Res*. 2014;6:149-170.
3. Crocetti E, Trama A, Stiller C, et al. Epidemiology of glial and non-glial brain tumours in Europe. *Eur J Cancer*. Jul 2012;48:1532-1542.
4. Grochans S, Cybulska AM, Simińska D, et al. Epidemiology of glioblastoma multiforme —literature review. *Cancers*. 2022;14:2412.
5. Hanif F, Muzaffar K, Perveen K, Malhi SM, Simjee SU. Glioblastoma multiforme: areview of its epidemiology and pathogenesis through clinical presentation and treatment. *Asian Pac J Cancer Prev*. 2017;18:3-9.
6. Sawlani V, Patel MD, Davies N, et al. Multiparametric MRI: practical approach and pictorial review of a useful tool in the evaluation of brain tumours and tumour-like lesions. *Insights Imaging*. 2020;11:84.
7. Abbasi AW, Westerlaan HE, Holtman GA, Aden KM, van Laar PJ, van der Hoorn A. Incidence of tumour progression and pseudoprogression in high-grade gliomas: a systematic review and meta-analysis. *Clin Neuroradiol*. 2018;28:401-411.
8. Thust SC, van den Bent MJ, Smits M. Pseudoprogression of brain tumors. *J Magn Reson Imaging*. 2018;48:571-589.
9. Hygino da Cruz LC Jr, Rodriguez I, Domingues RC, Gasparetto EL, Sorensen AG. Pseudoprogression and pseudoresponse: imaging challenges in the assessment of posttreatment glioma. *AJNR Am J Neuroradiol*. 2011;32:1978-1985.
10. Balaña C, Capellades J, Pineda E, et al. Pseudoprogression as an adverse event of glioblastoma therapy. *Cancer Med*. 2017;6:2858-2866.
11. Le Fevre C, Constans JM, Chambrelant I, et al. Pseudoprogression versus true progression in glioblastoma patients: a multiapproach literature review. Part 2 - radiological features and metric markers. *Crit Rev Oncol Hematol*. 2021;159:103230.
12. sindhumol SS, Balakrishnan K, Kumar A. Brain tissue classification from multispectral MRI by wavelet based principal component analysis. *Int J Image Graph Signal Process*. 2013;5:29-36.
13. Abdullah N, Lee WC, Ngah U, Ahmad K. *Improvement of MRI Brain Classification Using Principal Component Analysis*, 2011 IEEE International Conference on Control System, Computing and Engineering, Penang, Malaysia. 2011:557-561.
14. Jolliffe IT, Cadima J. Principal component analysis: a review and recent developments. *Philos Trans A Math Phys Eng Sci*. 2016;374:20150202.
15. Sun X, Shi L, Luo Y, et al. Histogram-based normalization technique on human brain magnetic resonance images from different acquisitions. *Biomed Eng Online*. 2015;14:73.
16. Amat J. *Análisis de Componentes Principales (Principal Component Analysis, PCA) y t-SNE*. Madrid, Spain: Ciencia de Datos; 2022.
17. Ding C, He X. *K-Means Clustering Via Principal Component Analysis*. ICML '04: Proceedings of the twenty-first international conference on Machine learning. 29. 2004.
18. Hartigan JA, Wong MA. Algorithm AS 136: a k-means clustering algorithm. *J R Stat Soc Ser C Appl Stat*. 1979;28:100-108.
19. Tibshirani R, Walther G, Hastie T. Estimating the number of clusters in a data set via the gap statistic. *J Roy Stat Soc B*. 2001;63:411-423.
20. Böhning D. Multinomial logistic regression algorithm. *Ann Inst Stat Math*. 1992;44:197-200.
21. Karschnia P, Vogelbaum MA, van den Bent M, et al. Evidence-based recommendations on categories for extent of resection in diffuse glioma. *Eur J Cancer*. 2021;149:23-33.
22. Bonavia R, Inda MM, Cavenee WK, Furnari FB. Heterogeneity maintenance in glioblastoma: a social network. *Cancer Res*. 2011;71:4055-4060.
23. Inda MM, Bonavia R, Seoane J. Glioblastoma multiforme: a look inside its heterogeneous nature. *Cancers*. 2014;6:226-239.
24. Parker NR, Khong P, Parkinson JF, Howell VM, Wheeler HR. Molecular heterogeneity in glioblastoma: potential clinical implications. *Front Oncol*. 2015;5:55.
25. Molina D, Perez-Beteta J, Luque B, et al. Tumour heterogeneity in glioblastoma assessed by MRI texture analysis: a potential marker of survival. *Br J Radiol*. 2016;89:20160242.
26. Brandsma D, Stalpers L, Taal W, Sminia P, van den Bent MJ. Clinical features, mechanisms, and management of pseudoprogression in malignant gliomas. *Lancet Oncol*. 2008;9:453-461.
27. Taal W, Brandsma D, de Bruin HG, et al. Incidence of early pseudo-progression in a cohort of malignant glioma patients treated with chemoirradiation with temozolomide. *Cancer*. 2008;113:405-410.
28. He J, Grossman RI, Ge Y, Mannon LJ. Enhancing patterns in multiple sclerosis: evolution and persistence. *AJNR Am J Neuroradiol*. 2001;22:664-669.
29. Feraco P, Donner D, Gagliardo C, et al. Cerebral abscesses imaging: a practical approach. *J Popul Ther Clin Pharmacol*. 2020;27:e11-e24.
30. Booth TC, Larkin TJ, Yuan Y, et al. Analysis of heterogeneity in T2-weighted MR images can differentiate pseudoprogression from progression in glioblastoma. *PLoS One*. 2017;12:e0176528.
31. Kim JY, Park JE, Jo Y, et al. Incorporating diffusion- and perfusion-weighted MRI into a radiomics model improves diagnostic performance for pseudoprogression in glioblastoma patients. *Neuro Oncol*. 2019;21:404-414.
32. Taylor C, Ekert JO, Sefcikova V, Fersht N, Samandouras G. Discriminators of pseudoprogression and true progression in high-grade gliomas: a systematic review and meta-analysis. *Sci Rep*. 2022;12:13258.
33. Hein PA, Eskey CJ, Dunn JF, Hug EB. Diffusion-weighted imaging in the follow-up of treated high-grade gliomas: tumor recurrence versus radiation injury. *AJNR Am J Neuroradiol*. 2004;25:201-209.
34. Lee WJ, Choi SH, Park CK, et al. Diffusion-weighted MR imaging for the differentiation of true progression from pseudoprogression following concomitant radiotherapy with

temozolomide in patients with newly diagnosed high-grade gliomas. *Acad Radiol*. 2012;19:1353-1361.

35. Matsusue E, Fink JR, Rockhill JK, Ogawa T, Maravilla KR. Distinction between glioma progression and post-radiation change by combined physiologic MR imaging. *Neuroradiology*. 2010;52:297-306.

36. Domínguez-Pinilla N, Martínez de Aragón A, Diéguez Tapias S, et al. Evaluating the apparent diffusion coefficient in MRI studies as a means of determining paediatric brain tumour stages. *Neurologia*. 2016;31:459-465.

37. Sugahara T, Korogi Y, Kochi M, et al. Usefulness of diffusion-weighted MRI with echo-planar technique in the evaluation of cellularity in gliomas. *J Magn Reson Imaging*. 1999;9:53-60.

38. Padhani AR, Liu G, Koh DM, et al. Diffusion-weighted magnetic resonance imaging as a cancer biomarker: consensus and recommendations. *Neoplasia*. 2009;11:102-125.

39. Khan AR, Khan S, Harouni M, Abbasi R, Iqbal S, Mehmood Z. Brain tumor segmentation using K-means clustering and deep learning with synthetic data augmentation for classification. *Microsc Res Tech*. 2021;84:1389-1399.

40. Qiao J, Cai X, Xiao Q, et al. Data on MRI brain lesion segmentation using K-means and Gaussian Mixture Model-Expectation Maximization. *Data Brief*. 2019;27:104628.

41. Wang X, Markowetz F, De Sousa EMF, Medema JP, Vermeulen L. Dissecting cancer heterogeneity–an unsupervised classification approach. *Int J Biochem Cell Biol*. 2013;45:2574-2579.

42. Khandwala K, Mubarak F, Minhas K. The many faces of glioblastoma: pictorial review of atypical imaging features. *NeuroRadiol J*. 2021;34:33-41.

43. Toga AW, Thompson PM. The role of image registration in brain mapping. *Image Vis Comput*. 2001;19:3-24.

44. Bauer S, Fejes T, Reyes M. A skull-stripping filter for ITK. *Insight J*. 2013;20:1-7.

45. Fortin JP, Sweeney EM, Muschelli J, Crainiceanu CM, Shinohara RT. Removing inter-subject technical variability in magnetic resonance imaging studies. *Neuroimage*. 2016;132:198-212.

46. Isaksson LJ, Raimondi S, Botta F, et al. Effects of MRI image normalization techniques in prostate cancer radiomics. *Phys Med*. 2020;71:7-13.

Conflict of interest statement: The authors declare that the article content was composed in the absence of any commercial or financial relationships that could be construed as a potential conflict of interest.

Received 1 July 2023; accepted 13 January 2024

Citation: World Neurosurg. (2024) 183:e953-e962. https://doi.org/10.1016/j.wneu.2024.01.074

Journal homepage: ***www.journals.elsevier.com/world-neurosurgery***

Available online: ***www.sciencedirect.com***